Untangling cosmic collisions: a study of particle acceleration and magnetic fields in merging galaxy clusters

Osinga, E.

1

Introduction

Just after the Universe came into being, it was an unimaginably small and hot soup of elementary particles, technically called a quark-gluon plasma (Adams et al., 2005). This soup was almost perfectly uniform, smoothed out by the postulated initial rapid expansion called inflation (Guth, 1981; Steinhardt, 1983; Linde, 1990) which likely ended before the universe was 10^{-32} seconds old. The fact that it was not perfectly uniform is predicted by quantum physics causing minute temperature fluctuations in the plasma.

As the Universe expanded more slowly after inflation, the extremely high density and temperatures started to decline, and when the Universe was a millionth of a second old, quarks combined into protons, neutrons and their antiparticle counterparts. After a full second, the Universe was cool enough that particles and antiparticles could annihilate each other and most of the energy in normal matter was converted to radiation. This marked the start of the radiation-dominated epoch of the Universe, which would last until the Universe is ~50,000 years old. During this period, the physics of everything is still rather simple, as the Universe consisted of an ionised plasma of predominantly protons, electrons, and photons forming an opaque plasma from which no light escapes. The interaction between photons and matter prevented the clumping of normal matter until after 380,000 years. Then, the Universe was cool enough for protons and electrons to finally combine into atoms for the first time (the event wrongfully termed "recombination") and the Universe became transparent. Dark matter, on the other hand, was not prevented from clumping by radiation, and could already freely grow from the initial energy density perturbations for the past 330,000 years. This has given the head-start on structure formation that is required to match the observed structure in the late-time Universe (e.g. Fig 1.1).

1.1 Large scale structure

The first radiation emitted after recombination can now be observed as the cosmic microwave background (CMB; e.g. Penzias & Wilson, 1965; Kogut et al., 1993; Hinshaw et al., 2009; Planck Collaboration et al., 2020a). The most recent observations of the CMB, made by the Planck satellite, provide strong support for the hot big bang model of an expanding Universe, with the tiny fluctuations generated by the inflationary period observed as slight temperature variations in the otherwise uniform background radiation (Planck

1

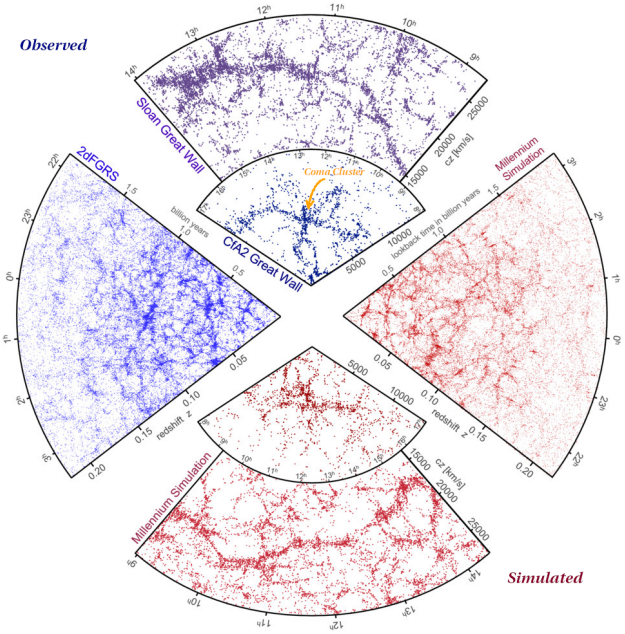

Figure 1.1: Distribution of the local large-scale structure of the Universe. The top half (in blue) shows the observed matter distribution, from three redshift surveys: CfA2 (Geller & Huchra, 1989), 2dFGRS (Colless et al., 2001) and SDSS (Gott et al., 2005). The Coma Cluster, one of the nearest and most massive clusters is indicated by the orange arrow. The lower half (in red) shows the simulated distribution from the Millenium simulations (Springel et al., 2005). Adapted from Springel et al. (2006).

Collaboration et al., 2020c). The concordance cosmological model, the ΛCDM model, fits these observations exquisitely, posing a Universe that consists, in terms of energy density, of 68% dark energy (Λ), 27% cold dark matter (CDM) and 5% ordinary baryonic matter (Planck Collaboration et al., 2020b). In the ΛCDM model, the clumped regions of dark matter, also called "haloes", grow hierarchically through accretion of matter and mergers with other haloes, described well by the Press-Schechter formalism (Press & Schechter, 1974; Lacey & Cole, 1993). As baryonic matter was accreted onto these halos, the first stars and galaxies formed by cooling and condensing gas (White & Rees, 1978). In turn, these galaxies aggregated into groups and clusters of galaxies, forming the large-scale structure as we observe it today. The gravitational collapse of the haloes can happen in all three spatial dimensions, usually first forming 2D "sheets" which collapse into 1D "filaments" which merge to form 0D "nodes" at the intersection between filaments. Most of the mass of the Universe is contained within these structures, while most of the volume of the Universe is occupied by the evolved versions of the initially underdense regions, now called voids.

Aligning structure

The described path of structure formation finally results in a filamentary matter distribution that looks like a *cosmic web* as shown in Figure 1.1. One of the largest cosmic structures is the Sloan Great Wall (Gott et al., 2005), a ~ 420 Mpc complex of superclusters. Although

not gravitationally bound, the Sloan Great Wall is a structure in the sense that it presents a network of connected matter aligning over cosmological scales. Because of their rarity, these largest scale structures present useful tests for the ΛCDM paradigm as they can constrain the initial fluctuation field or possibly challenge the uniformity of it (e.g. Sheth & Diaferio, 2011). Similarly, patterns in the orientation of galaxies within the large-scale structure can be used to test the cosmological model, since galaxies will be affected by the tidal forces imparted on them during structure formation (Codis et al., 2018; Kraljic et al., 2020). Extending this idea, the radio jets coming from active supermassive black holes (See Sect. 1.3) in the centres of galaxies could also be useful tools to trace the uniformity of the Universe on very large scales. A possible connection between radio jets and the large-scale structure of the Universe was implied by studies finding non-uniform jet orientations over large regions of the sky (Taylor & Jagannathan, 2016; Contigiani et al., 2017). However, small systematic effects in how the data was taken or analysed might result in significant non-uniformity and bias these results. Studies that incorporate redshifts to be less affected by such systematics, such as the study we perform in Chapter 2, have yet to conclusively find significant alignment of radio jets over large regions in the Universe (Panwar et al., 2020; Osinga et al., 2020; Simonte et al., 2023).

On slightly smaller scales, at the nodes of the cosmic web, where the filamentary structures meet each other, the largest gravitationally bound structures in the Universe are formed: galaxy clusters. These objects are the main focus of this thesis.

1.2 Galaxy clusters

Galaxy clusters are the most massive virialised objects to have formed from the merging of smaller haloes. They typically have masses[1] in the range $M_{500} = 10^{14} - 10^{15} M_{\odot}$, with dark matter making up 80% of the total mass (e.g. Vikhlinin et al., 2006). These large masses imply that clusters must have originated from large collapsing regions at high redshift, (radii of ~ 15 comoving Mpc at $z \sim 2$; Muldrew et al., 2015), which implies that clusters can be considered a representative sample of the Universe, in which the mean matter content is universal. This makes clusters an important laboratory for cosmology, as the number counts and gas mass fraction can be used to constrain cosmological parameters (e.g. Ettori et al., 2009; Planck Collaboration et al., 2016b). Clusters also provide important evidence for dark matter, with the most notable example being the Bullet Cluster (Clowe et al., 2004, 2006; Bradač et al., 2006; Paraficz et al., 2016, see also Fig. 1.2).

The intracluster medium

The galaxies inside a cluster make up only a few per cent of the total mass budget or roughly 10% of all the baryonic mass in a cluster. Most of the baryonic mass is contained in the hot ($\sim 10^7 - 10^8$ K or $\sim 1 - 10$ keV) and dilute ($10^{-2} - 10^{-4}$ particles cm^{-3}) plasma in the intracluster medium (ICM). Because of the extreme temperatures, the main cooling mechanism is thermal emission in the X-ray through optically thin bremsstrahlung (e.g. Forman & Jones, 1982). The characteristic spatial scales for density and temperature gradients are ~ 100 kpc, with clusters often showing a strongly rising density profile and steeply dropping temperature profile near their cores ($< 0.3 R_{500}$; Hudson et al., 2010). Given that the sound

[1] The mass is often expressed in terms of M_{500}, which is the mass enclosed in the radius R_{500}, where the density is 500 times the critical density of the Universe, but in principle, any number could be set here.

1

Figure 1.2: Composite image of the Bullet Cluster (NASA). Red shows the hot X-ray emitting baryonic gas, as observed by the Chandra X-ray observatory (Markevitch et al., 2002). Blue shows the distribution of matter as reconstructed from gravitational lensing (Clowe et al., 2004, 2006; Bradač et al., 2006; Paraficz et al., 2016), and the galaxies are shown in the background optical image from the Hubble Space Telescope (NASA,ESA) and the Magellan Telescope (University of Arizona). The baryonic gas clearly collided and is behind both the main mass component (i.e. dark matter) and the galaxies, which both did not collide.

speed in galaxy clusters is on the order of 10^3 km s^{-1}, typical disturbances take 10^8 years to cross these scales. In comparison, the mean free path of particles in the ICM is on the order of 10 kpc, so thermal particles collide only every 10^7 years. This means that the ICM must be treated as a weakly collisional fluid, complicating the magnetohydrodynamic (MHD) description (e.g. Kunz et al., 2012).

Gravity dominates the physics in galaxy clusters, and as a result, clusters are found to be relatively *self-similar*. This means that they have properties that simply scale with mass and redshift of the dark matter halo (e.g. Kaiser, 1986; Kravtsov & Borgani, 2012; Böhringer et al., 2012). This self-similarity holds for integrated properties such as temperature, X-ray luminosity and total mass (i.e. including baryons), as well as radial profiles of electron density, pressure and gas temperature (e.g. Croston et al., 2008; Arnaud et al., 2010a; Baldi et al., 2012). These relations do however show significant scatter in regions where baryonic physics becomes important, such as the cooling core region ($r < 0.3R_{500}$) and regions of infalling or accreting substructures (Ghirardini et al., 2019). Baryonic physics can thus contribute significantly to the virialisation process of clusters while presenting only less than 20% of the total mass budget. In particular, non-thermal pressure support from turbulence, bulk gas motions, magnetic fields and cosmic rays is found to be at the level of 10% of the total pressure support in local galaxy clusters (e.g. Eckert et al., 2019). Therefore, it is important to constrain non-thermal physics in galaxy clusters to get a full picture of structure formation, which is particularly relevant in the current era of precision cosmology (Turner, 2022).

Additionally, the ICM can be heavily perturbed by the interaction between clusters and their surrounding medium. Clusters are currently still forming and growing, through accretion of matter from their surroundings and mergers with other clusters. In fact,

mergers of massive clusters are the most energetic events since the Big Bang, able to release up to 10^{64} ergs (10^{57} joules) into the ICM on Gyr timescales. This energy is dissipated through weak shocks and turbulence, mainly heating the ICM (Markevitch & Vikhlinin, 2007). The turbulence is expected to be Kolmogorov-like (Kolmogorov, 1941), meaning that energy is transported from large scales to small scales with an energy spectrum of $E(k) \propto k^{-5/3}$ where k is the wavenumber (i.e. k=$2\pi/\ell$ with ℓ the physical scale). The scales on which turbulence is injected depend on the mechanism, with feedback from radio galaxies (Sect. 1.3) disturbing the ICM on scales of tens of kpc, to Mpc-scale injection during cluster mergers. In the relaxed (i.e. non-merging) Perseus cluster, the first direct measurements of turbulent motions were made by the Hitomi satellite (Hitomi Collaboration et al., 2016). These observations showed that the ICM of the Perseus cluster is fairly quiescent, with turbulent driving scales less than 100 kpc, consistent with AGN injected turbulence (Hitomi Collaboration et al., 2018).

Turbulence and shocks can also amplify magnetic fields and accelerate particles to relativistic energies on Mpc scales (Brunetti & Jones, 2014; van Weeren et al., 2019). Clusters thus provide a unique laboratory to study magnetic fields, particle acceleration and plasma physics on large scales and at high energies. Some fundamental physical questions include how particles are accelerated and heated in the ICM, what role large-scale magnetic fields play and how plasma physics affects the formation of the large-scale Universe. Radio observations of galaxy clusters are particularly well suited to answer these questions, as will be explained in the following sections.

1.3 Radio observations of galaxy clusters

Due to the highly dynamic nature of the ICM, galaxy clusters host a diverse range of interesting radio sources. In this thesis, when 'radio emission' is mentioned, it mainly means radio emission from frequencies of approximately 10 MHz to 10 GHz, which corresponds to wavelengths between 30 meters and 3 centimetres. Almost all of the radio emission received at these frequencies is synchrotron emission. Synchrotron emission occurs when charged particles[2] are accelerated in magnetic fields and emit radiation as they spiral along the field lines.

Radio galaxies

Although the galaxies only make up a few per cent of the total mass, the supermassive black holes in the centre of the galaxies can significantly impact the ICM (Fabian, 2012). If enough material is present surrounding a supermassive black hole, a hot accretion disk of infalling matter can form. Magnetic fields surrounding the accretion disk get strongly twisted, winding into a cone above the poles of the black hole. There, two opposite jets of relativistic plasma are launched, a process that can extract rotational energy from the black hole (e.g. Blandford & Znajek, 1977). These jets can stay collimated for tens or hundreds of kpc depending on the interaction between the jets and the ambient medium (Turner & Shabala, 2023). As the jet pushes into the ambient medium, it can form diffuse plumes or lobes. The relativistic electrons in the plasma emit synchrotron radiation, creating a radio galaxy (Fig 1.3) from an active galactic nucleus (AGN).

[2]We typically only see synchrotron emission from electrons as the power radiated is inversely proportional to the rest-mass to the power four and protons are ~ 2000 times heavier than electrons.

1

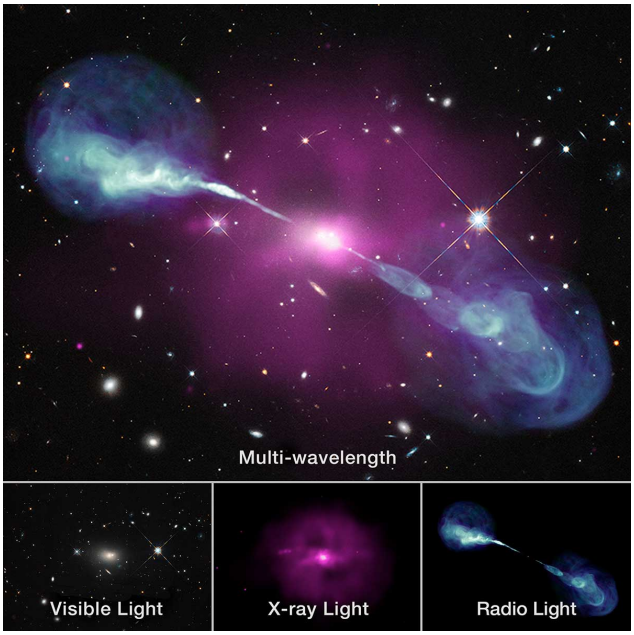

Figure 1.3: Multi-wavelength view of the radio galaxy Hercules A. In optical light, the galaxy hosting the supermassive black hole in the centre is visible. The hot gas surrounding the galaxy can be seen in X-rays, while the radio light reveals the large extended radio galaxy with collimated jets resulting in two lobes. Credit: X-ray: NASA/CXC/SAO; optical: NASA/STScI; radio: NSF/NRAO/VLA.

In galaxy clusters, the radio jets originating from AGN are often found to bend away from the direction of motion of the host galaxy as they are subject to ram pressure when moving through the ICM, causing *tailed* radio galaxies (e.g. Miley, 1980; Garon et al., 2019). When the tails are bent with a angles less than 90 degrees, they are typically called wide-angle tailed radio galaxies, while more extremely bent sources are called narrow-angle tailed radio galaxies (e.g. Fig. 1.4). The sizes of these sources can extend well beyond the host galaxy, with linear sizes from a few kpc up to a Mpc (e.g. Wilber et al., 2018). Additionally, with the advent of low-frequency telescopes such as the Low-Frequency Array (LOFAR, see Sect. 1.3.1), more examples are being found of old radio plasma that has lost a considerable amount of energy due to synchrotron and inverse Compton radiation, but is being re-energised through processes in the dynamic ICM (de Gasperin et al., 2017; van Weeren et al., 2017; Mandal et al., 2020).

Diffuse radio emission

On larger scales, radio observations of merging galaxy clusters have revealed that a large fraction of the volume of a cluster is filled with magnetic fields and ultra-relativistic electrons which can not be directly related to AGN activity (Feretti et al., 2012; van Weeren et al., 2019). This emission is generally labelled as *diffuse radio emission*, and it implies relativistic electrons with GeV energies (Lorentz factors of $\gamma > 10^3$) that spiral around μG magnetic fields in the clusters (Brunetti & Jones, 2014). Diffuse radio emission can be

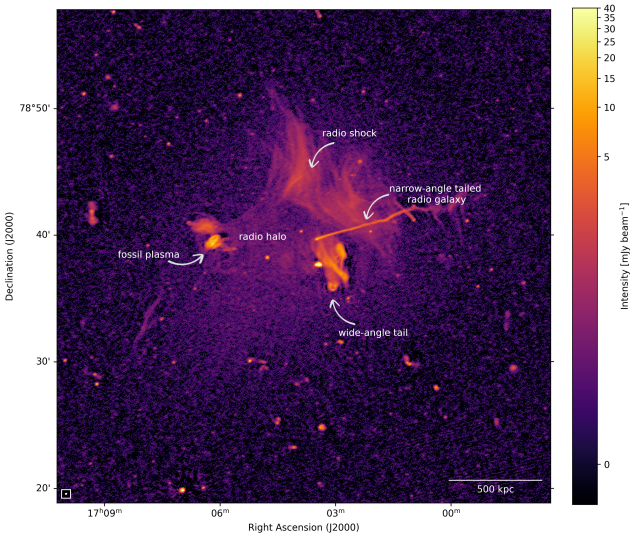

Figure 1.4: LOFAR 144 MHz image of the galaxy cluster Abell 2256 (Osinga et al., 2023a), with various types of radio emission annotated. The spherical region of enhanced radio emission near the centre is the radio halo, while the filamentary structure in the top right shows a radio shock. Various regular AGN are shown as point sources, as well as resolved bent-tailed radio AGN and re-energised plasma sources.

classified into two main categories. First, it includes radio halos, which are Mpc-sized regions of radio emission that are centrally located (e.g. Bonafede et al., 2022; Cuciti et al., 2022). Second, it comprises radio shocks (also called radio relics), which are elongated arc-shaped structures generally found on the outskirts of clusters. This thesis does not study radio shocks in detail, and therefore only a brief overview of radio shocks is presented. A more detailed introduction to radio halos and the relevant physics is given below.

Radio shocks

Radio shocks are observed about three times less frequently than radio halos in massive merging clusters (Botteon et al., 2022a), probably because they require a favourable orientation of the merger axis to be detected. The radio shocks are believed to trace merger-induced shock waves (Ensslin et al., 1998; Hoeft & Brüggen, 2007), and thus shock waves should be observable in the X-ray from temperature and density discontinuities in the ICM. These discontinuities are most easily observed if the merger is in the plane of the sky. In many cases, shock waves, co-located with radio shocks, are indeed observed in the X-ray (e.g. Tab. 2 in van Weeren et al., 2019). Due to high compression at the shock front, the turbulent magnetic field in the ICM is expected to be amplified and aligned with the propagating plane of the shock (Ensslin et al., 1998). This should result in linearly polarised emission, confirmed by observations at GHz frequencies often finding polarisation fractions of $10-50\%$ (e.g. Di Gennaro et al., 2021c; Rajpurohit et al., 2022a).

In an idealised case of a merger between two massive unperturbed clusters, it is expected that at the first encounter, two equatorial shocks are launched perpendicular to the merging axis as the ICM is compressed along the merger axis. Subsequently, two axial shocks, often

simply called merger shocks, are launched in opposite directions along the merger axis (e.g. Ha et al., 2018; Lee et al., 2020). Equatorial shocks are difficult to observe as they are less energetic than merger shocks, and in fact, only one has been observed (Gu et al., 2019). Merger shocks are typically observed on the outskirts of galaxy clusters (e.g. van Weeren et al., 2016a; Hoang et al., 2017), which agrees with simulations finding that the kinetic energy through the shocks peaks roughly 1 Gyr after shock launching, because the Mach number and shock surface area grow faster than the ICM density decreases (Vazza et al., 2012; Ha et al., 2018). This results in shocks that are typically brightest $\gtrsim 1$ Mpc from the centre of galaxy clusters.

In reality, the turbulent nature of the ICM causes a complex shock front that is composed of many shocks with different Mach numbers. Radio observations are more sensitive to the high Mach number shocks with efficient electron acceleration, while X-ray observations probe the average Mach number of the shock front (Wittor et al., 2021). Both wavelengths are thus needed to understand the complex dynamics and particle acceleration within shocks in the ICM.

Radio halos

Radio halos are characterised by low surface brightness radio emission ($\sim \mu$Jy arcsec^{-2} at 1 GHz frequencies) that generally follows the baryonic distribution of the ICM, thus being brightest at the centre of the cluster (e.g. Giovannini et al., 1993; Feretti et al., 1997a,b; Giacintucci et al., 2005; Clarke & Ensslin, 2006; Rajpurohit et al., 2018; Hlavacek-Larrondo et al., 2018; Botteon et al., 2020b; Bonafede et al., 2022). The radiation typically has a steep spectrum ($\alpha < -1$; van Weeren et al., 2019, with $S \propto \nu^{\alpha}$, where ν denotes the frequency and S the flux density) and is thus significantly brighter at low frequencies. In contrast to the high degree of polarisation of radio shocks, radio halos are almost always completely unpolarised. Three studies have claimed polarised emission from radio halos (Govoni et al., 2005; Bonafede et al., 2009; Girardi et al., 2016), but a clear detection remains elusive as the polarised signal might be related to shocks seen in projection (Pizzo et al., 2011; Rajpurohit et al., 2021a). Although radio halos should be intrinsically polarised, the turbulent nature of the ICM causes strong Faraday rotation and depolarisation (See also Sect. 1.4.2) near the centre of clusters preventing a clear detection (Govoni et al., 2013; Loi et al., 2018, 2019; Sur et al., 2021). The large size of radio halos implies that the relativistic electrons cannot all be generated at a single location in the cluster (e.g. the centre) and diffuse outwards. The typical lifetime of a GeV electron in a μG magnetic field is less than 10^8 yr given synchrotron and inverse Compton losses (van Weeren et al., 2019), while the time required for these electrons to cover Mpc distances is orders of magnitude larger ($10^9 - 10^{10}$ yr) given typical ICM bulk or plasma diffusion velocities of 10^2 km s^{-1} (Bagchi et al., 2002). This is known as the diffusion problem and requires some type of in-situ acceleration of electrons to solve (Jaffe, 1977). The two main models proposed to solve the diffusion problem for radio halos are the hadronic model and the turbulent re-acceleration model.

Hadronic model

The hadronic model states that the relativistic electrons are secondary products of collisions between cosmic ray protons (CRp) and thermal protons (e.g. Dennison, 1980; Blasi et al., 2007; Blasi & Colafrancesco, 1999), which circumvents the diffusion problem because relativistic protons have lifetimes larger than the age of the Universe and can thus easily

accumulate and distribute throughout the ICM. CRp should be present to some degree in the ICM, injected by AGN (e.g. Shi et al., 2022) and accelerated by shock waves and turbulence (e.g. Wittor, 2021). Once generated, CRp are basically confined to the cluster forever (~ 10 Gyr; Brunetti & Jones, 2014), though these cannot be directly detected. However, the presence of CRp should result in γ-ray emission from decay products of the hadronic interactions. The decay chain should go as follows (e.g. Blasi & Colafrancesco, 1999)

$$p + p \rightarrow \pi^0 + \pi^+ + \pi^- + \text{other} \tag{1.1}$$

$$\pi^0 \rightarrow \gamma\gamma \tag{1.2}$$

$$\pi^\pm \rightarrow \mu^\pm + \nu_\mu/\bar{\nu}_\mu \rightarrow e^\pm + \nu_e/\bar{\nu}_e + \bar{\nu}_\mu/\nu_\mu, \tag{1.3}$$

where the proton-proton collisions produce neutral and charged pions. The neutral pions quickly decay into gamma rays, while the charged pions decay into muons and muon neutrinos, which are also unstable and decay into cosmic ray electrons (or positrons).

This model thus poses a possible solution for generating relativistic electrons throughout the cluster volume, with a relatively straightforward prediction for the amount of gamma-ray emission from neutral pion decay. However, despite more than two decades of searches, such a γ-ray signal has not yet conclusively been detected (Reimer et al., 2003; Ackermann et al., 2014, 2015). So far, upper limits on the gamma-ray emission have ruled out the purely hadronic model for the nearest most massive cluster (Coma cluster; Brunetti et al., 2012). Although recently a gamma-ray signal was detected from the Coma Cluster by the Fermi Large Area Telescope (Xi et al., 2018; Adam et al., 2021; Baghmanyan et al., 2022), it is not clear whether the signal is associated with the ICM. Tentative evidence pointed towards the emission being extended, in line with a signal from the ICM, but due to the limited resolution of Fermi-LAT possible contamination of AGN could not be ruled out. However, even assuming that the signal can be fully attributed to the ICM, the purely hadronic model was still ruled out for the Coma Cluster and the CRp were constrained to encompass less than 2% of the thermal energy within R_{500} (Adam et al., 2021).

Another argument against proton-proton collisions being the main fueling mechanism of radio halos is the existence of radio halos with ultra-steep spectra ($\alpha < -1.5$) (Brunetti et al., 2008). Producing such a steep spectrum through hadronic collisions requires a steep spectrum for the CRp energy distribution as well, which integrated over the cluster volume would imply energy densities of CRp that are of the same order as the thermal energy density. Other than this scenario being unrealistic given the knowledge of the thermal properties of the ICM and pressure balance, ultra-steep spectrum radio halos would then also produce a large amount of γ-rays, strongly violating γ-ray upper limits (Ackermann et al., 2014, 2015).

Turbulent re-acceleration

The turbulent re-acceleration model poses to solve the diffusion problem by in-situ stochastic acceleration of electrons. Stochastic acceleration, also called Fermi-II-type acceleration (Fermi, 1949), occurs in any magnetised medium with random motions (i.e. turbulence). As a charged particle randomly collides with magnetised clouds in the ICM, it can either gain or lose energy depending on if the collision was head-on or tail-on. For any particle moving in a particular direction surrounded by randomly moving magnetised clouds, a

head-on collision is more likely than a tail-on collision and thus particles are, on average, accelerated in a turbulent medium.

This process is likely important in the ICM, as a fraction of the energy injected by cluster mergers is channelled into turbulence, fueling the pursuit of various models of turbulent acceleration (Brunetti & Blasi, 2005; Brunetti & Lazarian, 2016, 2011; Pinzke et al., 2017). However, because of the stochastic nature, Fermi-II acceleration is rather inefficient and the acceleration of thermal electrons is not sufficient to produce radio halos (Petrosian & East, 2008). The proposed solution is therefore *re-acceleration* of supra-thermal, or mildly relativistic, electrons. This requires a large rather uniform population of supra-thermal electrons throughout the cluster volume, and their origin is still uncertain (e.g. Nishiwaki & Asano, 2022). It is possible that these seed electrons are injected into the ICM by AGN (Vazza et al., 2021), or that they are leftovers from previous merger events. Alternatively, they could be produced by the hadronic model, which might more naturally explain the distribution throughout the cluster volume.

The turbulent re-acceleration model is currently the favoured model to explain radio halos, owing to various successful predictions. The model naturally predicts a connection between radio halos and mergers, which has been firmly established observationally (Cassano et al., 2010b; Wen & Han, 2013; Cuciti et al., 2015; Cassano et al., 2023). In this model, radio halos are expected to show a radio spectrum that steepens after some frequency ν_s set by the balance between acceleration and energy losses (Cassano et al., 2010a). Ultra-steep spectra can thus be observed at $\nu \geq \nu_s$, explaining ultra-steep spectrum radio halos which cannot exist in the purely hadronic scenario. The turbulent energy available, ultimately set by the mass and mass ratio of the merger should correlate with ν_s, making radio halos in low-mass clusters more easily observable at lower frequencies. Indeed, observations with low-frequency telescopes in mass-selected samples are now clearly finding a connection between radio halo occurrence and cluster mass (Cuciti et al., 2021a,b). Finally, the spatial distribution of the spectral index across radio halos is often patchy and disordered and shows a sub-linear point-to-point correlation with X-ray emission, consistent with a turbulent acceleration scenario with inhomogeneous conditions across the cluster volume (e.g. Botteon et al., 2020b; Bonafede et al., 2022; Rajpurohit et al., 2023).

1.3.1 Instrument: The Low Frequency Array

The study of particle acceleration and diffuse radio emission is best performed at low frequencies, as can be appreciated from the predictions of the turbulent re-acceleration model, and the generally steep radio spectra of the diffuse radio emission. The low-frequency instrument of choice for this thesis is the Low-Frequency Array (LOFAR; van Haarlem et al., 2013). LOFAR is the largest low-frequency radio interferometer to date, with baseline lengths of over 1000 km. It consists of 52 stations, spread out over eight countries in Europe, although more stations are planned. At the time of writing, the collaborative countries and distribution of stations are as follows: the Netherlands (38 stations), Germany (six stations), Poland (three stations), France (one station), Ireland (one station), Latvia (one station), Sweden (one station) and the United Kingdom (one station). Stations are planned also in Italy and Bulgaria. All stations comprise two types of antennas, the Low-Band Antennas (LBA) and the High-Band Antennas (HBA). The HBA antennas work in the frequency range of 110-240 MHz while the LBA antennas work down to the

lowest ground-based observable frequency (10-90 MHz). Below approximately 10 MHz, the ionosphere reflects radio waves back into space, preventing observations from Earth. Above 10 MHz, the ionosphere still significantly refracts radio waves, altering them by causing time delays, amplitude variations and rotation of the polarisation angle. Because the ionosphere is highly variable in space and time, different stations see differently distorted waves, requiring advanced direction-dependent calibration at high time and frequency resolution to make science-quality images (van Weeren et al., 2016b; de Gasperin et al., 2019, 2020; Tasse et al., 2021). Ionospheric distortions scale inversely with frequency, which is why LOFAR observations have been mainly focused on the HBA band, with sky surveys such as the LOFAR Two-metre Sky survey (LoTSS; Shimwell et al., 2017, 2019, 2022) leading the way. LoTSS is mapping the whole northern sky between $120-168$ MHz at $6''$ resolution to a noise level below $100\,\mu$Jy beam^{-1}. It has currently detected over 4 million radio sources, and is expected to detect ~ 15 million once complete.

Recent advances in calibration and imaging techniques are also significantly opening up the sub-100 MHz sky. The LBA counterpart to LoTSS is the LOFAR LBA Sky Survey (LoLSS; de Gasperin et al., 2021, 2023), being performed at the most sensitive part of the LBA band, $44-66$ MHz. A new, more experimental, survey has very recently started to explore the lowest frequency window from $10-30$ MHz, i.e. where wavelengths reach 10 meters or larger. This survey aims to cover the entire northern sky above 20° declination (where sources can be observed at favourable elevations), and is called the LOFAR Decametre Sky Survey (LoDeSS). Remarkably, in just over two years, the observations have already covered the proposed sky area due to the incredibly large field-of-view of LOFAR stations (> 200 deg^2) at these long wavelengths, and the multi-beam functionality of a digital telescope such as LOFAR. Whether this data can be reduced and imaged with the same success as LoLSS and LoTSS still remains to be seen, but science-quality images have recently been made at decametre wavelengths (Osinga et al., 2023a; Groeneveld et al., 2023), providing an optimistic outset.

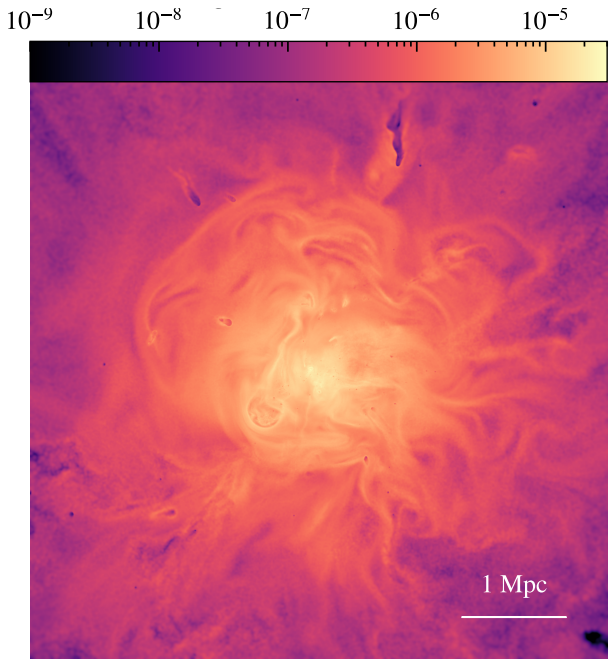

Figure 1.5: The magnetic field strength (in G) and structure as observed in an extremely high resolution cosmological zoom-in simulation centred on a massive galaxy cluster. The image shows a slice of 100 kpc thickness. The field is clearly ordered on many different scales, from kpc up to Mpc scales. Image credit: U. Steinwandel (2023).

1.4 Cluster magnetic fields

Magnetic fields permeate the Universe on a wide range of scales, spanning from the $\sim$ 100 Gauss magnet on the fridge and the $\sim$ 1G magnetic field surrounding the Earth to the $\sim 5\times10^{-6}$ G magnetic field in our galaxy (e.g. Haverkorn, 2015). These fields extend to Mpc scales in galaxy clusters (e.g. Osinga et al., 2022) and are thought to exist at nano-Gauss levels on even larger scales in the intergalactic medium (e.g. Amaral et al., 2021). Although the origin and evolution of these Mpc scale magnetic fields, or cosmic magnetic fields, are one of the major mysteries in astrophysics, theoretical work and simulations show that if a very weak seed field ($< 10^{-10}$ G) is present, small-scale dynamo processes can amplify the fields to μG values in galaxy clusters (Ryu et al., 2008; Vazza et al., 2014, 2018; Donnert et al., 2018; Steinwandel et al., 2022). For the origin of the seed field, two main hypotheses have been proposed (Cho, 2014). The magnetic fields could be primordial in origin, arising in the early Universe before recombination or during structure formation (Widrow et al., 2012). Alternatively, cosmic magnetic fields could also be seeded from astrophysical processes. Supernovae, galactic outflows and AGN can inject magnetised material into the intergalactic medium which can then be transported to larger scales (Rees, 2006). Both mechanisms could be important, and the degree of influence they have on the final magnetic field is an important ingredient for simulations of magnetic field amplification (e.g. Donnert et al., 2018).

Magnetic fields in galaxy clusters can have a significant impact on energy transport in the ICM, possibly suppressing Kelvin-Helmholtz instabilities that would otherwise form at the boundaries between hot and cold gas during a merger or disruption event (ZuHone et al., 2011, 2015). Virtually all models of cosmic ray acceleration also depend crucially on the magnetic field properties of clusters (Brunetti & Jones, 2014). However, not much is known about the properties of present-day magnetic fields in galaxy clusters.

Magnetic field strength

The strength is the best-constrained property of cluster magnetic fields, estimated to be in the range of $1-10\mu$G, from equipartition estimates from diffuse radio emission (e.g. Stroe et al., 2014; Giovannini et al., 1993, i.e assuming that the total energy density of the relativistic plasma is equally divided between cosmic rays and magnetic fields, which is similar to the minimum energy condition) and Faraday rotation experiments (e.g. Murgia et al., 2004; Govoni et al., 2006; Guidetti et al., 2008; Bonafede et al., 2010; Vacca et al., 2010, 2012; Govoni et al., 2017; Stuardi et al., 2021), which will be explained in more detail in the next section. In principle, cluster magnetic field strengths can also be constrained from X-ray observations. Inverse Compton scattering of low-energy CMB photons off of the relativistic electrons in the ICM should create a non-thermal power-law of X-ray emission on top of the thermal bremsstrahlung (e.g. Sarazin & Kempner, 2000). However, such a measurement has never been confirmed unambiguously, resulting in sub-μG lower limits on the volume averaged magnetic field strength in clusters (Wik et al., 2014; Gastaldello et al., 2015; Cova et al., 2019; Rojas Bolivar et al., 2021; Tümer et al., 2023). A tentative detection was made recently (Mirakhor et al., 2022), but more data is needed to confirm this.

Magnetic field structure

The structure of the cluster magnetic field remains elusive, with studies finding power spectra of magnetic field fluctuations with exponent n in the range of $n = 2$ to $n = 4$ (assuming they follow a power-law, e.g. Murgia et al., 2004; Govoni et al., 2006; Guidetti et al., 2008; Bonafede et al., 2010; Vacca et al., 2010, 2012; Govoni et al., 2017). This is roughly consistent with the Kolmogorov expectation of incompressible turbulence, which yields a power-law with $n = 3.67$ (Kolmogorov, 1941). The minimum and maximum scales on which this power-law holds is also not well-constrained but should follow the turbulence length scales. Turbulence can be injected on many different scales, from kpc scales due to AGN feedback and galactic outflows, up to Mpc scales during major cluster mergers (e.g. Fig 1.5). The smallest scales can be probed with high-resolution polarisation studies of nearby objects, such as the nearby brightest cluster galaxy Cygnus A, where it was found that the magnetic field shows fluctuations on sub-kpc scales (Sebokolodi et al., 2021). The largest scales are more difficult to probe and require a statistical analysis of many independent sight-lines (e.g. Osinga et al., 2022), or polarised structures that span the scale of the cluster (e.g. Govoni et al., 2005).

Dependence on cluster properties

Finally, it is unclear how the magnetic field properties depend on cluster properties such as mass, dynamical state, temperature or redshift. While clusters are remarkably self-similar in their thermal properties (see Sect. 1.2), the self-similarity of their non-thermal properties

is not well established. There are simulations that show that there is a fixed ratio of energy components in clusters throughout a cluster's history, with gravitational energy mostly being dissipated into thermal energy, then turbulent energy and finally magnetic energy (Miniati & Beresnyak, 2015). Observationally this is less clear, as in some cases extreme mergers are found with significantly increased non-thermal pressure (e.g. Ghirardini et al., 2018).

The magnetic field strength B is often assumed to scale with the electron density n_e as $B = B_0 \left(\frac{n_e(r)}{n0}\right)^{\eta}$ (e.g. Bonafede et al., 2010), where B_0 denotes the central magnetic field strength. This strength is frequently set independently of the central electron density n_0. However, a possible scaling between B_0 and n_0 was observed in a small compiled sample of clusters studied in the literature (Govoni et al., 2017), indicating also some self-similarity in the magnetic field properties. However, larger samples of homogeneously selected and analysed clusters are needed to confidently assert such a scaling.

The evolution of cluster magnetic fields as a function of cosmic time is also not well-constrained, due to the difficulty of observing clusters at high redshifts. However, LOFAR observations of a small sample of radio halos in high-redshift ($z = 0.6 - 1.0$) galaxy clusters (Di Gennaro et al., 2021a,b, 2023) have shown that clusters already have similar μG magnetic field strengths when the Universe was half its age. This implies that magnetic field amplification happens early during cluster formation, indicating that the magnetic field amplification process must be efficient and fast.

1.4.1 Instrument: The Karl G. Jansky Very Large Array

Radio polarisation observations of Faraday rotation and depolarisation, induced by the magnetised ICM, present the most promising tool for studying magnetic fields. Polarised studies are best performed at GHz frequencies because sources depolarise very quickly towards lower frequencies. At GHz frequencies, there is a good balance between sources still being polarised and the fractional bandwidth of the observations being large enough that their polarised properties can be determined accurately. The instrument of choice to study magnetic fields in this thesis is the Karl G. Jansky Very Large Array (VLA; Thompson et al., 1980).

The VLA is a radio interferometer located in New Mexico (United States), that was built between 1973 and 1980. In contrast to LOFAR which only consists of antennas, the VLA consists of 27 dishes 25 meters in diameter that can in principle observe between 73 MHz and 50 GHz. The dishes are on rail tracks shaped in a "Y" which allows different telescope configurations. The largest configuration gives a longest baseline of 36 km, resulting in a maximum resolution of $1.3''$ in the L-band ($1 - 2$ GHz).

1.4.2 Technique: Faraday rotation and depolarisation

Faraday rotation is the rotation of the polarisation angle of light caused by birefringent properties of a magnetised plasma. The observed rotation of the polarisation angle is strongly wavelength dependent,

$$\chi(\lambda) = \chi_0 + \mathrm{RM}\,\lambda^2, \tag{1.4}$$

with χ denoting the polarisation angle, λ the wavelength and RM the *rotation measure*. In the case of a simple emitting source located behind a screen of magnetised plasma

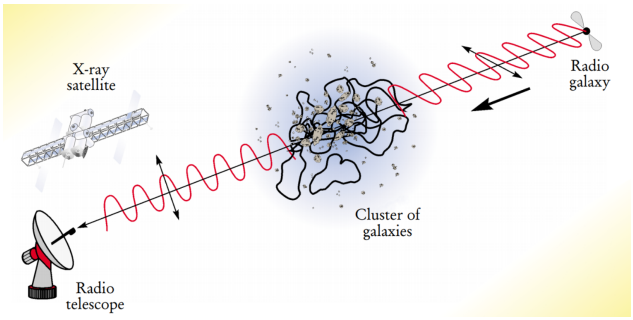

Figure 1.6: Illustration of a Faraday rotation experiment. A radio galaxy is emitting polarised synchrotron radiation with a certain intrinsic polarisation angle. As the wave hits the magnetised plasma inside the cluster, the angle is rotated depending on the wavelength according to Eq. 1.4. By measuring the rotation with a radio telescope, and the plasma density with an X-ray satellite, the magnetic field of the plasma can be obtained. Credit: Philipp P. Kronberg, Physics Today, December 2002

(e.g. a radio source behind a cluster, see Fig 1.6), the RM is equal to the more generalised Faraday depth (ϕ). The Faraday depth of a source is directly proportional to the line-of-sight component of the magnetic field weighted by the electron density as (Burn, 1966; Brentjens & de Bruyn, 2005)

$$\phi(\mathbf{r}) = 812 \int n_e \mathbf{B} \cdot d\mathbf{r} \, \mathrm{rad\,m^{-2}}, \tag{1.5}$$

where $\mathbf{B}$ is the magnetic field vector in units of μGauss, n_e is the electron density in particles per cm^{-3} and d$\mathbf{r}$ the infinitesimal path length increment in kpc, oriented along the line of sight. Generally, a magnetic field pointing towards the observed is defined with $\phi(\mathbf{r}) > 0$.

If the magnetised screen itself also emits polarised radio emission along the line of sight, Equation 1.5 still holds but the interpretation becomes a bit more complex. Now, a single line of sight can have multiple Faraday depth values, or even an extended Faraday depth structure if the screen has an appreciable thickness along the line of sight. In general, we observe (Burn, 1966)

$$P(\lambda^2) = \int_{-\infty}^{+\infty} F(\phi) e^{2i\phi\lambda^2} d\phi, \tag{1.6}$$

where P and F denote the polarised intensity as a function of wavelength or Faraday depth, respectively. This equation is similar to a Fourier transform, except that only ϕ can take unbounded values while λ^2 is positive by definition, and not measured at all values of $\lambda^2 > 0$. Still, it is possible to invert this equation given some assumptions, in a process called RM synthesis (Brentjens & de Bruyn, 2005). This allows an estimate of the Faraday dispersion function $F(\phi)$. If the wavelength coverage is good enough (analogous to uv-coverage in interferometry), polarised emission at different Faraday depths along the line of sight can be separated.

By combining radio observations of polarised sources with X-ray data, which provides insights into the thermal electron densities, it is thus possible to study the magnetic fields in galaxy clusters using Eq 1.5. Unfortunately, most radio sources are observed to be unpolarised. A typical VLA observation in the L-band of 1 hour only detects about 6 polarised sources over the entire field-of-view (e.g. Osinga et al., 2022). The number count of

polarised sources is also weakly dependent on polarised flux density F_p, as $N(> F_p) \propto F_p^{-0.6}$ (Rudnick & Owen, 2014), i.e. observing for 4 times longer only results in 1.5 times more sources.

There are several mechanisms that can cause depolarisation of radio sources. First, random fluctuations in the magnetic field across the emitting source will cause different intrinsic polarisation angles, thus causing intrinsic depolarisation that is wavelength independent. Second, internal depolarisation can occur when a radio source is emitting at different Faraday depths along the line of sight (i.e. the medium producing the synchrotron emission is also doing the Faraday rotation). Third and most important in the context of this thesis, there is external depolarisation if the magnetised plasma that constitutes the foreground screen is highly turbulent, as in the case of galaxy clusters. Because interferometers have a finite resolution (restoring beam size), we measure the sum of many waves along slightly offset sightlines which have picked up different Faraday depths and thus interfere destructively.

To illustrate the magnitude of the external depolarisation in the case of galaxy clusters, imagine a simple scenario of a constant magnetic field in the ICM with a random orientation in cells of size Λ_c kpc. The observed RM (Eq. 1.5) then results from a random walk process. Because of the central limit theorem, the distribution of RMs is expected to tend towards a Gaussian with zero mean, and variance given by (e.g. Murgia et al., 2004)

$$\sigma^2_{\rm RM} = 812^2 \Lambda_c \int (n_e B_{\parallel})^2 dl, \tag{1.7}$$

where $B_{\parallel}$ is the magnetic field strength parallel to the line of sight in μG. Observing this variance within a single resolution element causes a dramatic reduction of the polarisation fraction p (e.g. Burn, 1966) that goes as

$$p = p_0 \exp(-2\sigma^2_{\rm RM}\lambda^4), \tag{1.8}$$

where p_0 denotes the intrinsic polarisation fraction of the source. As both the magnetic field strength and electron densities generally increase towards the centre of clusters, we are expected to observe more and more depolarised sources, which has indeed been observed and can be used to constrain cluster magnetic field parameters (Bonafede et al., 2011; Osinga et al., 2022).

1.5 This thesis

This thesis starts by investigating the anisotropy of the large-scale structure using the LOFAR Two-metre Sky Survey, because previous studies have found that radio jets tend to align across large portions of the sky (Sect. 1.1). If confirmed, this would have significant implications for large-scale structure formation in the Universe. Subsequently, the thesis focuses on understanding the physics of particle acceleration and magnetic fields in galaxy clusters. While considerable advances have been made in understanding the non-thermal properties of galaxy clusters, there are still significant gaps in our knowledge.

Diffuse radio emission is almost exclusively found in high mass clusters, owing to more energetic mergers simply producing more luminous radio emission. However, the most massive clusters are the rarest density peaks in the Universe, while less massive clusters

($M_{500} < 5 \times 10^{14} M_{\odot}$ often used as a boundary) are much more common (e.g. Böhringer et al., 2017). Knowledge of particle acceleration is currently thus limited to the tip of the iceberg of the cluster population. In less massive clusters, with smaller turbulent energy budgets, turbulent re-acceleration may become less important, and hadronic interactions might power low-luminosity radio halos (Cassano et al., 2012; Brunetti & Jones, 2014). Due to the expected steep spectrum and faint nature of radio emission in lower mass clusters, deep radio observations at low frequencies are required.

Studies on magnetic field properties in galaxy clusters are still in their infancy, with only a handful of individual clusters studied so far (Murgia et al., 2004; Govoni et al., 2006; Guidetti et al., 2008; Bonafede et al., 2010; Vacca et al., 2010, 2012; Govoni et al., 2017; Stuardi et al., 2021; Anderson et al., 2021). These studies form an inhomogeneously selected sample of clusters, analysed with varied approaches, prohibiting general conclusions on magnetic field properties. Typically, each study observes fewer than five polarized radio sources, and these radio galaxies are often embedded within the intracluster medium (ICM). As a result, a question arises regarding whether these studies truly investigate the magnetized ICM or if they attribute polarization variations, which may be local to the radio sources, to the properties of the ICM.

In this thesis, we aim to answer the following questions:

- Are the angles of radio jets aligned over large scales in the Universe, possibly tracing anisotropy in the large-scale structure? (**Chapter 2**)
- Do lower mass clusters also host radio halos, and are their properties in line with radio halos observed in higher mass clusters? (**Chapter 3**)
- Is it possible to calibrate and image LOFAR observations down to the lowest frequency window of 10-30 MHz, and if so, is there a new population of diffuse cluster radio sources that can be uncovered? (**Chapter 4**)
- What are the properties of the magnetic fields in nearby and massive galaxy clusters? (**Chapter 5,6**)

In **Chapter 2**, the alignment of the jets of radio galaxies over cosmological scales is investigated. We compiled a sample of 7,555 double-lobed radio galaxies from the first data release of the LOFAR Two-metre Sky Survey to test the null hypothesis that their jet angles are randomly distributed across angular (2D) and physical (3D) scales. The results showed a significant departure from a random distribution of angles on scales of about four degrees on the sky, implying the observed jet angles align across large regions. However, no such alignment signal was found in a 3D analysis using the sub-sample of 4,212 sources to which a redshift could be attributed. Additionally, the alignment effect correlated strongly with an apparent source property, radio flux density, instead of a physical property such as radio power. The results thus pointed towards the interpretation that the alignment effect is caused by an unknown systematic bias in the data, rather than a physical alignment.

In **Chapter 3**, a systematic search for diffuse radio emission in low-mass galaxy clusters is carried out. We analysed the deepest images ever made at 150 MHz as part of the LOFAR Two-metre Sky Survey Deep fields, which reached noise levels below 30 μJy beam^{-1} at

$6''$ resolution. These observations revealed a new high-redshift radio halo at $z = 0.77$ in a relatively low mass cluster ($M_{500} = 3.3^{+1.1}_{-1.7} \times 10^{14} M_{\odot}$) and a tentative radio halo detection in another low mass cluster, Abell 2201 ($M_{500} = 2.67^{+0.27}_{-0.26} \times 10^{14} M_{\odot}$). Deep upper limits on other low-mass clusters that showed no diffuse radio emission were set. Although the sample size was relatively small, results were consistent with the known relation between radio halo power and cluster mass, extrapolated down to lower masses.

In **Chapter 4**, LOFAR is pushed to the limit as we observe the nearby galaxy cluster Abell 2256 down to the extremely low frequency of 16 MHz. LOFAR images between 16 and 168 MHz were presented, filling in the last unexplored window of Abell 2256. We detected and resolved the filamentary radio shock, radio halo and various ultra-steep spectrum sources. By adding in literature data at higher frequencies, we measured the integrated radio spectrum of the radio halo between 24 and 1500 MHz, and the radio shock between 24 and 3000 MHz. Both classes of diffuse emission showed single power-law spectra, with the radio halo being significantly steeper ($\alpha = -1.56 \pm 0.02$) than the radio shock ($\alpha = -1.00 \pm 0.02$). A new fossil plasma source was also detected with an extremely steep spectrum of $\alpha = -1.9 \pm 0.1$. Finally, the purely hadronic model was ruled out for Abell 2256 by combining the radio data with 13.5 years of γ-ray observations from the Fermi Large Area Telescope.

In **Chapters 5 and 6**, VLA observations of 124 Planck clusters from the *Chandra-Planck Legacy Program for Massive Clusters of Galaxies* are presented. The aim of these observations was to statistically infer the magnetic field properties of galaxy clusters through a stacking experiment. By stacking all clusters, 819 polarised radio sources were found, providing a relatively dense sampling of sight lines through clusters. **Chapter 5** presents the analysis of the depolarisation of radio sources in this sample. For the first time, a clear trend was detected of background sources increasingly depolarising as their projected radius to the cluster centre decreases. Using X-ray data from Chandra to constrain the electron densities, theoretical models with magnetic fields treated as Gaussian random fields were compared to the data. The data were best described by models with a central magnetic field strength of $5 - 10\,\mu$G and power-law indices between $n = 1$ and $n = 4$. **Chapter 6** improves this analysis by adding the information from the Faraday rotation of the sources. We observed a clear increase in the scatter of rotation measures towards the centre of galaxy clusters, consistent with an average magnetic field strength on the order of 3μG. Combining the depolarisation and rotation measure and comparing to a full forward model, the best agreement was found for an average magnetic field with a central strength of 5μG and a thermal gas density scaling of $B \propto n_e^{0.5}$. The power spectrum of the magnetic field was found to be consistent with the expectation from Kolmogorov turbulence, with maximum fluctuation scales of over 300 kpc, implying turbulence injected on large scales.

1.6 Future outlook

The detection of gravitational waves (Abbott et al., 2016) and the first image of a black hole (Event Horizon Telescope Collaboration et al., 2019) are compelling examples of the fact that scientific breakthroughs often come from technological advances. At the time of writing this thesis, major technological advances in radio astronomy are on the horizon, with the Square Kilometre Array (SKA) as the culmination. Even before the SKA becomes

operational, many projects will improve our understanding of the non-thermal content of galaxy clusters.

LOFAR will undergo a big upgrade to LOFAR2.0 (e.g. Edler et al., 2021), which involves upgrading the electronics of all the stations and a synchronized clock system for the Dutch stations. Currently, LOFAR can only observe in either the LBA or the HBA, and LBA observations can only utilise 48 out of the 96 LBA dipole antennas that are present per station. The electronics upgrade will allow the use of 144 dipoles simultaneously, thus allowing all LBA antennas and HBA antennas to observe at the same time. Combined with the synchronised clock system that will reduce phase errors, the upgrade is expected to improve the LBA imaging sensitivity by roughly a factor of five. Even as the SKA comes online, LOFAR will be the only telescope able to make high-resolution images below 100 MHz, which will offer a unique view of lower energy acceleration processes, particularly in low-mass clusters. LOFAR2.0 will be an important step in uncovering the origin of the seed pool of relativistic electrons that is thought to be present throughout the ICM. In addition, the new WEAVE spectrograph on the William Herschel Telescope on La Palma, currently doing commissioning observations, will take over a million spectra of bright LOFAR-selected radio sources (Smith et al., 2016). This will allow the study of (proto-)cluster radio galaxies at high redshift but also provide a large dataset to test radio galaxy alignment in three dimensions with majorly improved number statistics.

At GHz frequencies, precursors of the SKA such as MeerKAT (Jonas & MeerKAT Team, 2016) and The Australian Square Kilometre Array Pathfinder (ASKAP; Schinckel et al., 2012) will revolutionise our view of the magnetised universe. MeerKAT observations have a significantly larger field-of-view and higher sensitivity than VLA observations at the same frequency, due to the larger number of smaller-sized dishes operating at a lower system temperature (MeerKAT has 64 dishes of 13.5-meter diameter, while the VLA has 27 dishes of 25 meters in diameter). MeerKAT will thus be a great tool for deep polarisation studies of individual galaxy clusters with tens of polarised background sources detected per cluster. This will enable the study of detailed radial magnetic field profiles, potentially without assuming spherical symmetry. It will provide valuable information about the degree of self-similarity of magnetic fields in clusters.

ASKAP consists of 36, 12 meter dishes able to observe between $700 - 1800$ MHz. One of the surveys ASKAP is currently undertaking is the Polarization Sky Survey of the Universe's Magnetism (POSSUM; Gaensler et al., 2010), where early results are already showing interesting cluster science for both magnetic fields and particle acceleration (Anderson et al., 2021; Loi et al., 2023). However, the real power of POSSUM will come from the fact that it will observe the entire sky south of $+30^{\circ}$, resulting in a grid of polarised sources with an expected density of 25 deg^{-1}, which is 25 times higher than the currently best grid available from the NRAO VLA Sky Survey (NVSS; Condon et al., 1998). With at least 1397 massive clusters detected by Planck (Planck Collaboration et al., 2016a) in the survey area, this will yield unprecedented statistics for studying magnetic fields as a function of cluster properties and stacking towards the outskirts of clusters and filaments, where the magnetic field is poorly constrained. Together with the ongoing Very Large Array Sky Survey (VLASS; Lacy et al., 2020) covering the northern sky, unparalleled constraints will be set on the strength and structure of magnetic fields in the intergalactic medium, providing crucial input for cosmic magnetogenesis models.

Further in the future, in the first phase of the SKA project, the higher frequency antennas (SKA1-mid, > 350 MHz) might already be sensitive enough to detect polarisation in radio halos (Loi et al., 2019). This would allow highly detailed studies of magnetic fields and turbulence in the ICM. The lower frequency antennas (SKA1-low, < 350 MHz) will allow much greater samples of diffuse emission up to high redshifts. SKA1-low might even be able to finally constrain the contribution of the hadronic model by directly detecting radio halos in relaxed galaxy clusters with low levels of turbulence (Cassano et al., 2015). As the SKA becomes fully operational, the study of the non-thermal properties of clusters will undergo a transformation, and only time will tell what we will discover about the Universe.